[5] E. N. Skomal, "Theory of operation of a 3-port Y-junction ferrite circulator," *IEEE Trans. Microwave Theory Tech.*, vol. MTT-11, pp. 117–122, Mar. 1963.
[6] B. Owen, "The identification of modal resonances in ferrite loaded waveguide Y-junctions and their adjustment for circulation," *Bell Syst. Tech. J.*, vol. 51, pp. 595–627, Mar. 1972.
[7] J. B. Davies, "An analysis of the m-port symmetrical H-plane waveguide junction with central ferrite post," *IRE Trans. Microwave Theory Tech.*, vol. MTT-10, pp. 596–604, Nov. 1962.
[8] N. Tsukamoto, M. Suzuki, and T. Matsumoto, "An analysis of the waveguide Y-junction with ferrite," *Trans. Inst. Electron. Commun. Eng. Jap.*, vol. 54-B, pp. 131–138, Apr. 1971.
[9] S. Nakahara and H. Kurebayashi, "Circulator performance improvement by scattering matrix method," Paper Tech. Group on Microwaves, Inst. Electron. Commun. Eng. Jap., Dec. 1963.
[10] K. K. Chow, "On the solution and field pattern of sylindrical and dielectric resonators," *IEEE Trans. Microwave Theory Tech.* (Corresp.), vol. MTT-14, p. 439, Sept. 1966.
[11] Y. Kobayashi, "The resonators applied on strip lines," Paper Tech. Group on Microwaves, Inst. Electron. Commun. Eng. Japan., Jan. 1971.
[12] R. F. Harrington, *Time-Harmonic Electromagnetic Fields*. New York: McGraw-Hill, 1961.
[13] N. Ogasawara and T. Noguchi, "Modes identification of a dielectric triangular post resonator," to be presented at the 1974 Nat. Conv. Institute of Electrical Engineers of Japan.
[14] S. A. Schelkunoff, *Electromagnetic Wave*. New York: Van Nostrand.

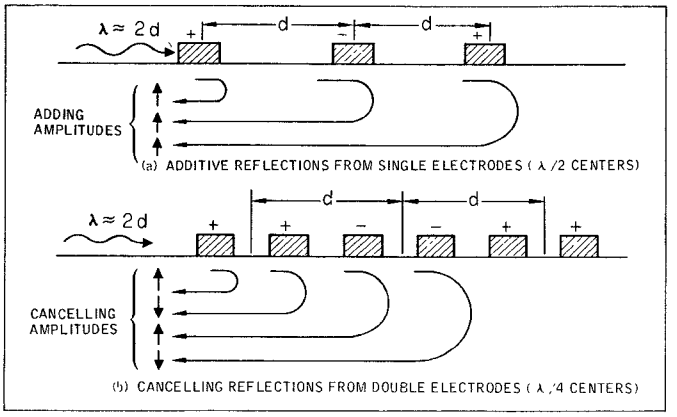

Fig. 1. Mass/electrical loading reflections of single and double electrodes.

Experimental Distinction Between Crossed-Field and In-Line Three-Port Circuit Models for Interdigital Transducers

W. RICHARD SMITH

***Abstract*—The crossed-field and in-line Mason circuit models for interdigital surface-wave transducers give opposite predictions for the dependence of acoustic reflection coefficients on electric load resistance for purely resistive loads. Experiments described herein show that the crossed-field model correctly describes the reflections for YX quartz, ST-X quartz, and YZ lithium niobate substrates. A low-resistance load minimizes reflections for transducers with double electrodes operating at the fundamental synchronous frequency. For single electrode transducers, optimum reflection suppression may call for a load resistance comparable to the transducer impedance.**

I. INTRODUCTION

The crossed-field and in-line three-port Mason circuits [1] for bulk-wave transducers have found wide usage as approximate equivalent circuits for interdigital surface-wave transducers [2]. Arguments for preferring both the in-line and crossed-field models have been suggested by various authors [3]–[6]. In addition, an intermediate mixed model has been proposed by Milsom and Redwood [7]. In [8] some differences between the models are emphasized, and it is stated that the choice of model apparently depends on the piezoelectric substrate.

This short paper provides an experimental basis for determining which model gives the better representation of a particular interdigital transducer and piezoelectric substrate. In addition, it negates a statement made earlier in [8] to the effect that the two models predict identical results for *all* transducer three-port transfer properties in the weak-coupling limit. The new finding reported here is that measurements of transducer acoustic reflection coefficients as a function of electric load resistance can determine which model is applicable, since the two models predict opposite behavior for purely resistive loads. Specific results are given in the following for "double electrode" [9] transducers on YX quartz, ST-X quartz, and YZ lithium niobate, and for a "single electrode" transducer on YZ lithium niobate.

II. ACOUSTIC REFLECTIONS

The experimental distinction between the crossed-field and in-line Mason circuits is based on measuring the acoustic reflection coefficient of a transducer as a function of the electric load. We begin by distinguishing the two causes of surface-wave reflections in interdigital transducers.

The first cause is the fact that metal electrodes short out the tangential electric field at the crystal surface and introduce mechanical loading, so that the electrode and gap regions have different apparent wave impedances [10], [11]. The second cause is that forward and backward surface waves are "regenerated" in the transducer by the voltage that the incident surface wave delivers to the electric load. The magnitude of the regenerated surface waves can be reduced (at a sacrifice in insertion loss) by varying the load impedance.

In ordinary single electrode transducers [Fig. 1(a)], the "mass/electrical loading" (MEL) reflections can become particularly troublesome because the metal stripes are spaced by one-half wavelength, causing MEL reflections to add in phase. The double electrode geometry [9] [Fig. 1(b)] provides a high degree of cancellation of the MEL reflections from successive electrodes, so that the reflections in double electrode devices are almost entirely of the regenerated wave (RW) type. Our purpose here is to determine a transducer circuit model which accurately describes the total (MEL and RW) reflections with particular emphasis on their relation to the electric load.

III. MASON CIRCUIT MODELS

The Mason circuits for bulk-wave transducers have found wide usage in surface-wave work since they give a three-port description of interdigital transducers, either periodic or dispersive with many nonidentical electrodes. In order to account for the different acoustic-wave impedances of the electrode and gap regions, the circuit of Fig. 2 has been used by at least two authors [10], [11]. In this circuit the unit cell of length d is subdivided into a metallized and an unmetallized region, with wave impedances Z_m and Z_0 in the corresponding acoustic transmission lines.

Synchronous operation is defined by the condition that d be equal to one-half acoustic wavelength ($\lambda = 2d$), and the circuit of Fig. 2

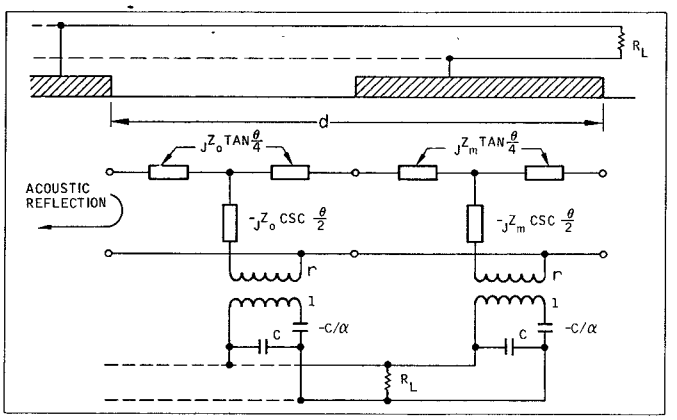

Fig. 2. Mason circuit model for single electrodes, including an acoustic-wave impedance discontinuity.

Manuscript received March 13, 1974; revised June 13, 1974. This work was sponsored by the U. S. Army Electronics Command, Fort Monmouth, N. J., under Contract DAAB07-73-C-0175.
The author is with Hughes Aircraft Company, Fullerton, Calif. 92634.

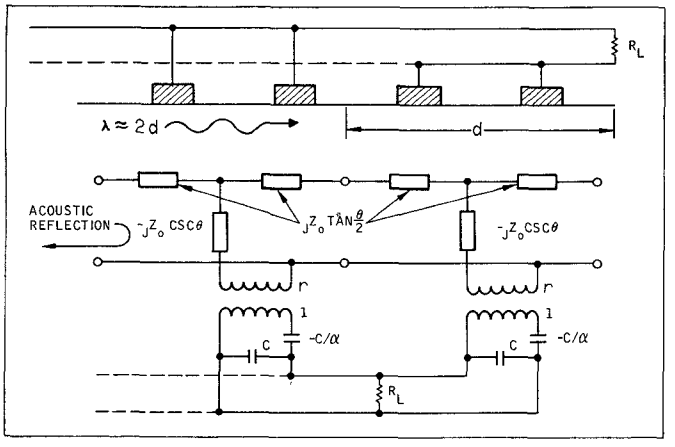

Fig. 3. Mason circuit without impedance discontinuity for double electrodes (assumes perfect cancellation of MEL reflections).

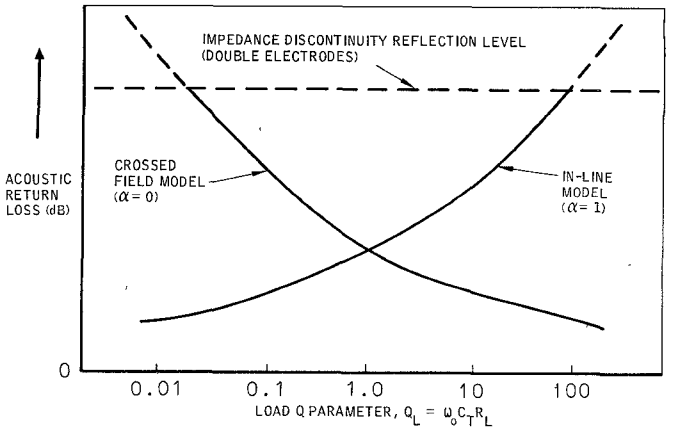

Fig. 4. Schematic of acoustic return-loss predictions of crossed-field and in-line Mason circuit models without impedance discontinuity.

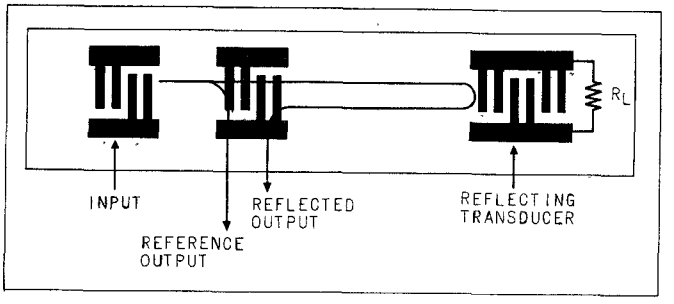

Fig. 5. Schematic of delay line for measuring acoustic return loss.

corresponds to single electrodes. By means of the parameter α the circuit can be designated as the "crossed-field" model [2] ($\alpha = 0$), the "in-line" model [2] ($\alpha = 1$), or the "mixed" model [7] ($0 < \alpha < 1$).

Up to the present time we have not modified the Mason circuits to distinguish between the electric- and acoustic-field distributions of single and double electrodes. We have, however, modeled the effect of double electrodes on MEL reflections by including in the region of length *d four* Mason circuits of like electric polarity but of alternating wave impedances Z_0 and Z_m. For operation near the synchronous condition $\lambda = 2d$, this circuit will exhibit a high degree of cancellation of MEL reflections of successive metal stripes, while maintaining the electric driving period of one acoustic wavelength. However, to emphasize the nearly total cancellation of MEL reflections by double electrodes near acoustic synchronism, we will adopt the approximate circuit of Fig. 3, in which we assign the same acoustic-wave impedance Z_0 to both the electrode and gap regions. Thus *for double electrodes we consider acoustic reflections to be entirely of the RW type*, i.e., due to the presence of, and controlled by, the electric load. This model is accurate as long as the RW reflections are not so small as to be comparable to the low residual MEL reflection level of a double electrode grating. In effect, the double electrodes enable us to study RW reflections alone.

As indicated schematically in Figs. 2 and 3, we consider the case of a purely resistive load in this experiment. The primary reason for choosing this case is the striking fact that the crossed-field ($\alpha = 0$) and in-line ($\alpha = 1$) Mason circuit models predict *completely opposite dependence of the RW reflection level on the load resistance.* In fact, for operation at the acoustic synchronous frequency with a resistive load, the acoustic return loss of a transducer is given in decibels by

$$L_{11} = -10 \log_{10}\left[\frac{\alpha^2 + Q_L^2(\alpha - 1)^2}{(\alpha + Q_L Q_r)^2 + (Q_r + [1 - \alpha]Q_L)^2}\right]. \quad (1)$$

The parameter Q_r is the transducer "radiation Q," i.e., the ratio of transducer capacitive susceptance to the synchronous acoustic radiation conductance. The variable is the "load Q"

$$Q_L = \omega_0 C_T R_L \quad (2)$$

which is just the load resistance normalized by the transducer susceptance.

A schematic plot of the acoustic return loss is given in Fig. 4, where the value of Q_r is not specified and exact values are not assigned to the ordinate scale. The parameter Q_r depends on the transducer geometry and substrate electromechanical coupling constant. The effect of varying Q_r is to shift the L_{11} curves up and down without disturbing the following behavior. The *crossed-field model* ($\alpha = 0$) calls for a *low-resistance load* to minimize RW reflections (i.e., to maximize the acoustic return loss L_{11}). On the other hand, the *"in-line" model* calls for a *high-resistance load* to achieve the same goal. The horizontal dashed line in Fig. 4 indicates that even with double electrodes there is a small residual MEL reflection and the solid curves (which describe RW reflections only) are not valid above this dashed line.

IV. EXPERIMENT

Inasmuch as the crossed-field and in-line circuit models predict opposite dependence of RW reflections on load resistance, an experimental distinction between the two models can be made by measuring acoustic return loss versus load resistance for double electrode transducers. A test delay line (shown schematically in Fig. 5) contains two short broad-band transducers for launching and detecting surface waves and one longer transducer, with electric load R_L, whose reflection coefficient is to be measured. The incident signal consists of an RF pulse long enough to "fill" the transducer under test, with the carrier set at the acoustic synchronous frequency. The load resistor is inside the mounting box to minimize parasitic capacitance, inductance, and resistance in the leads between the transducer and the load. Electrode resistance can be measured and counted as part of the load resistance R_L. The transducers are spaced to allow easy resolution of the reference output and reflected output pulses. The acoustic return loss is obtained by comparing the reference and reflected output pulses with the appropriate correction for propagation loss and reduction of the incident wave in its first pass under the detecting transducer.

Measurements of the acoustic return loss were carried out for double electrode transducers operating at 50 MHz on three different substrates: YX quartz, ST-X quartz, and YZ lithium niobate. Load resistances ranged from an open circuit down to a short directly stitch bonded across the transducer terminals. Intermediate resistors were connected across the transducer with minimal lead length, entirely inside the mounting box without feedthrough connectors.

V. RESULTS

Fig. 6 shows the theoretical and experimental values of acoustic return loss for a 100-period transducer on YX quartz. Note the virtually perfect agreement between the measured data and the crossed-field circuit model. The highest return loss (48 dB) was obtained with a stitch-bonded short-circuit load, where the effective load resistance is the resistance of the transducer electrodes and the wire bonds. Even at this low reflection level, the reflection is essentially a regenerated wave from the load, since this grating suppresses MEL reflections by 62 dB. That figure represents the limit of suppression on YX quartz, which could be obtained with a short-circuit

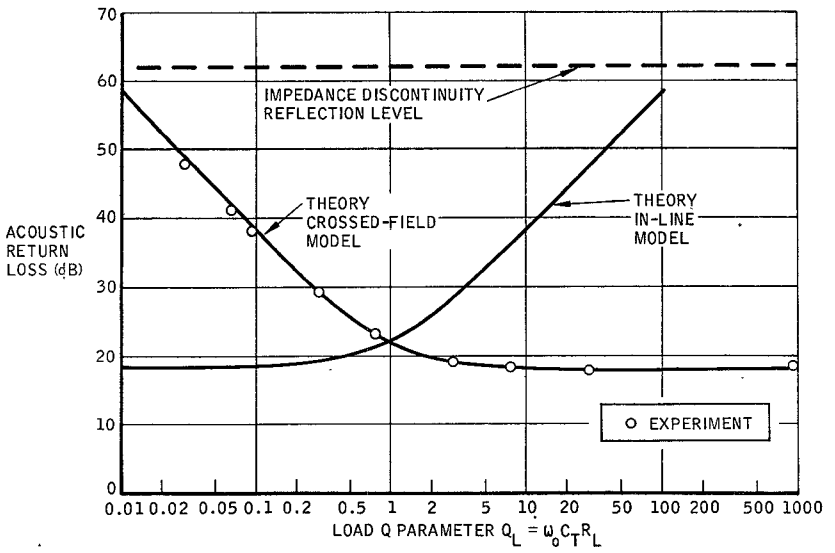

Fig. 6. Theoretical and experimental acoustic return loss for a 100-period double electrode transducer on YX quartz.

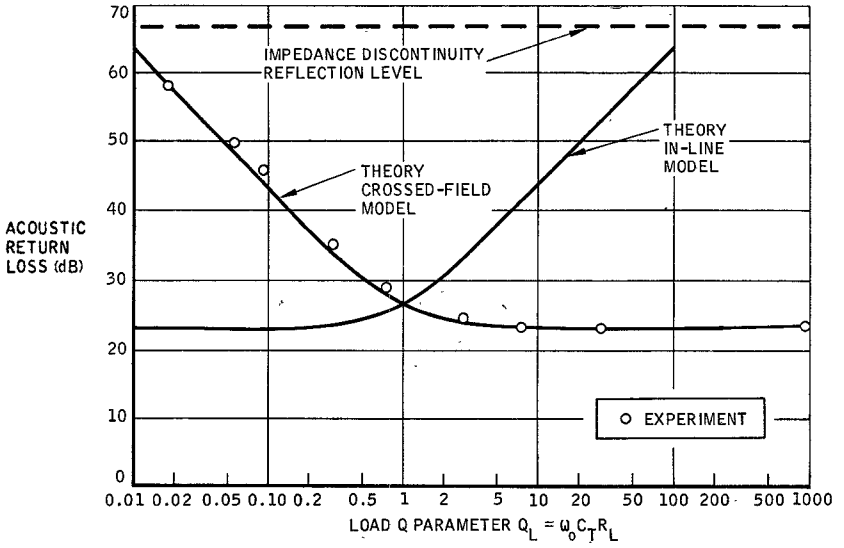

Fig. 7. Theoretical and experimental acoustic return loss for a 100-period double electrode transducer on ST-X quartz.

load if there were no resistance in the transducer electrodes and wire bonds.

A similar result is found for a 100-period transducer on ST-X quartz, as evidenced by the data of Fig. 7. In this case the grating suppresses MEL reflections by 67 dB so that the observed reflections are again entirely regenerated waves from the electric load. The crossed-field model again gives an excellent description of the observed behavior. The highest acoustic return loss, obtained with a stitch-bonded short circuit, is 58 dB.

The higher dielectric and electromechanical coupling constants of YZ lithium niobate made an 8-period transducer convenient for the acoustic return-loss measurement. Therefore, the theoretical curves (which ignore MEL reflections) are expected to be valid only for acoustic return loss up to 30 or 35 dB. The agreement between the experiment and the crossed-field theory is again quite good (see Fig. 8) except for some deviation above 30-dB suppression where MEL reflections become important. We have not recalculated the theoretical curve with the inclusion of different acoustic-wave impedances in the electrode and gap regions.

In modeling the acoustic reflections of *single* electrode transducers, it is obviously necessary to assign different wave impedances to the electrodes and gaps, since MEL reflections from successive electrodes tend to add rather than cancel. The foregoing results suggest retention of the crossed-field model with the addition of the different wave impedances, as in Fig. 2, with $\alpha = 0$. In order to test this model, we have made reflection measurements on an untuned 25-period single electrode transducer on YZ lithium niobate. Fig. 9 compares the measured acoustic return loss of this transducer against the prediction of the crossed-field model with impedance discontinuity, assuming $Z_0/Z_m = 1.018$, where Z_0 and Z_m are the acoustic-wave impedances of the gaps and electrodes, respectively.

The crossed-field model with impedance discontinuity correctly predicts that high acoustic return loss cannot be obtained with either a high- or low-resistance load. For $Q_L \gg 1$, RW reflections dominate and for $Q_L \ll 1$, MEL reflections dominate. The highest return loss (only about 8 dB) is obtained for an intermediate load resistance, where there is apparently a partial cancellation of MEL and RW reflections. Also shown for reference is the crossed-field theory without the impedance discontinuity, i.e., the acoustic return loss that would be expected if MEL reflections were not important.

VI. CONCLUSIONS

It is well known that double electrodes are desirable whenever they are allowed by fabrication constraints, since they nearly eliminate MEL reflections and allow the designer to achieve high acoustic return loss (at a sacrifice in insertion loss) by varying the load resistance. The foregoing results show that maximum return loss is

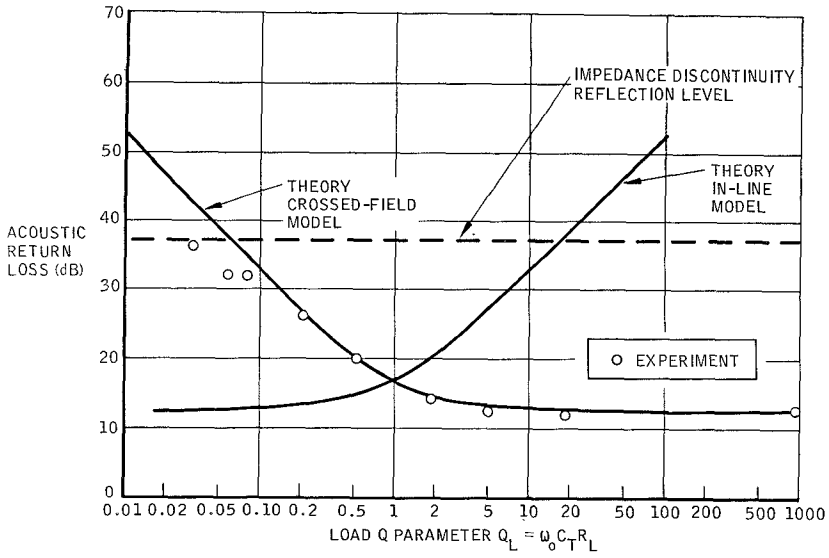

Fig. 8. Theoretical and experimental acoustic return loss for an 8-period double electrode transducer on YZ lithium niobate.

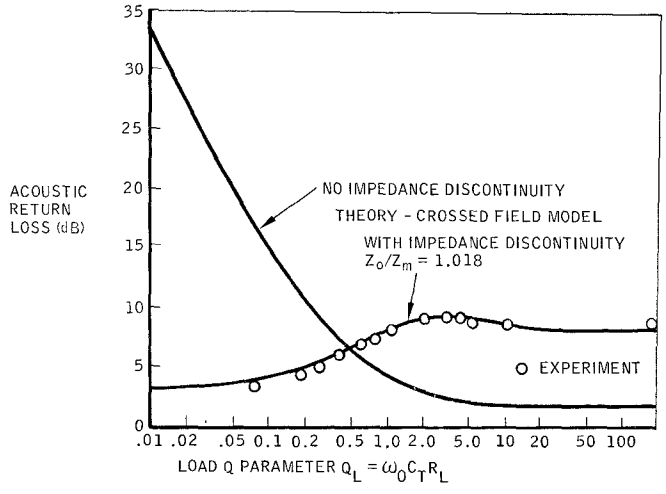

Fig. 9. Theoretical and experimental acoustic return loss for a 25-period single electrode transducer on YZ lithuim niobate.

obtained with a *low*-resistance load as predicted by the *crossed-field* circuit model in double electrode devices on YX quartz, ST-X quartz, and YZ lithium niobate substrates.

The crossed-field model also appears to give a good description of acoustic return loss in single electrode transducers if different acoustic-wave impedances are assumed for the electrode and gap regions. However, for single electrodes, MEL reflections limit the degree to which a low-impedance load can improve (increase) the return loss, and maximum return loss may occur for an intermediate impedance load rather than for the lowest possible load impedance.

The ordinary crossed-field model (even with different acoustic-wave impedances in the electrode and gap regions) [10], [11] is based on a spatial distribution of electric and acoustic fields for bulk waves [1] rather than surface waves. For this reason, its successful application to surface waves has largely been confined to fundamental frequency (rather than higher harmonic) operation. In addition, it does not fully account for the effects of varying stripe-to-gap width ratios. Considerable work has already been accomplished [12]–[14] to overcome these difficulties. The implication of the present results is that any circuit model modifications for this purpose should retain the $\alpha = 0$ (short-circuited or "absent" negative capacitor) feature of the crossed-field model, at least for the substrates and unity stripe-to-gap width ratios considered here. The experiment described here can be repeated (if desired) for other piezoelectric substrates and also for different stripe-to-gap width ratios to determine whether the in-line [2] ($\alpha = 1$) or mixed [7] ($0 < \alpha < 1$) model might in some cases give the best description of the load-induced acoustic reflections.

REFERENCES

[1] W. P. Mason, *Electromechanical Transducers and Wave Filters*, 2nd ed. Princeton, N. J.: Van Nostrand, 1948, pp. 201–209, 399–409.
[2] W. R. Smith, H. M. Gerard, J. H. Collins, T. M. Reeder, and H. J. Shaw, "Analysis of interdigital surface wave transducers by use of an equivalent circuit model," *IEEE Trans. Microwave Theory Tech.* (*Special Issue on Microwave Acoustics*), vol. MTT-17, pp. 856–864, Nov. 1969.
[3] T. Krairojananan and M. Redwood, "Piezoelectric generation and detection of ultrasonic surface waves by interdigital electrodes: An electrical equivalent circuit," *Electron. Lett.*, vol. 5, pp. 134–135, Apr. 3, 1969.
[4] R. F. Mitchell, W. Willis, and M. Redwood, "Electrode interactions in acoustic surface wave transducers," *Electron Lett.*, vol. 5, pp. 456–457, Sept. 18, 1969.
[5] L. T. Claiborne, C. S. Hartmann, and W. S. Jones, "Annual technical report for surface wave devices," Texas Instruments, Inc., pp. 63–68, Jan. 15, 1969–Jan. 15, 1970.
[6] R. F. Mitchell, "The interdigital transducer: Current state of theory," presented at the 1971 IEEE Ultrasonics Symp., Paper G-1.
[7] R. F. Milsom and M. Redwood, "Interdigital piezoelectric Rayleigh wave transducer: An improved equivalent circuit," *Electron. Lett.*, vol. 7, pp. 217–218, May 1971.
[8] W. R. Smith and H. M. Gerard, "Differences between in-line and crossed-field three-port circuit models for interdigital transducers," *IEEE Trans. Microwave Theory Tech.* (Corresp.), vol. MTT-19, pp. 416–417, Apr. 1971.
[9] T. W. Bristol, W. R. Jones, P. B. Snow, and W. R. Smith, "Applications of double electrodes in acoustic surface wave device design," in *1972 IEEE Ultrasonics Symp. Digest*, pp. 343–345.
[10] W. R. Smith, H. M. Gerard, and W. R. Jones, "Analysis and design of dispersive interdigital surface-wave transducers," *IEEE Trans. Microwave Theory Tech.*, vol. MTT-20, pp. 458–471, July 1972.

[11] W. S. Jones, C. S. Hartmann, and T. D. Sturdivant, "Second order effects in surface wave devices," *IEEE Trans. Sonics Ultrason.*, vol. SU-19, pp. 368–377, July 1972.
[12] R. Krimholtz, "Equivalent circuits for transducers having arbitrary asymmetrical piezoelectric excitation," *IEEE Trans. Sonics Ultrason.*, vol. SU-19, pp. 427–436, Oct. 1972.
[13] A. J. Bahr and R. E. Lee, "Equivalent circuit model for interdigital transducers with varying electrode widths," *Electron. Lett.*, vol. 9, pp. 281–282, June 28, 1973.
[14] C. S. Hartmann and B. G. Secrest, "End effects in interdigital surface wave transducers," in *Proc. 1972 IEEE Ultrasonics Symp.*, pp. 413–416.

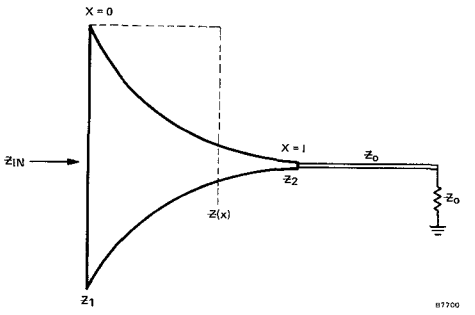

Fig. 1. An exponentially tapered transmission line loaded at the high impedance end with Z_0.

Normalized Impedance Graphs for Exponential Transmission Lines

ROBERT P. ARNOLD, MEMBER, IEEE, WILLIAM L. BAILEY, MEMBER, IEEE, AND RIMANTAS L. VAITKUS, MEMBER, IEEE

***Abstract*—Sign errors in an existing closed form solution for the reflection coefficient along an exponentially tapered transmission line have been corrected and the solution has been modified by the use of electrical line length. This allows useful graphs for the input impedance of the tapered line to be computed which are normalized with respect to frequency and system impedance. The graphs clearly demonstrate both the broad-band and narrow-band properties of the tapered line.**

INTRODUCTION

Numerous articles [1]–[6] have been published on the analysis and application of exponentially tapered transmission lines. However, relatively few authors have published graphs which materially aid in their application. Ramachandran [7] developed three independent charts for obtaining the locus of the input reflection coefficient of an exponential line terminated in a resistance equal to the impedance level at that end. However, these charts must be used in conjunction with the Smith chart for the evaluation of the input impedance. Kamnitis [8] presented a curve on the impedance characteristics of an exponential taper as a function of frequency. However, this curve was for only one impedance transformation ratio.

The purpose of this short paper is to present a useful graphical representation of the input impedance to the exponentially tapered transmission line for various impedance transformation ratios normalized with respect to frequency and the system characteristic impedance. Both the familiar broad-band and the less well-known narrow-band properties of the tapered line will be clearly illustrated.

ANALYSIS

Fig. 1 shows an exponentially tapered transmission line used with a system whose characteristic impedance is Z_0. The high impedance end of the taper (Z_2) is connected to a line of characteristic impedance Z_0, which in turn is terminated in a real load of Z_0, or driven by a generator of impedance Z_0. The defining equation for the characteristic impedance of the tapered line is given by

$$Z(X) = Z_1 \exp(\delta X) \tag{1}$$

where

Z_1 line impedance at the low impedance end;
δ taper rate per unit distance ≥ 0;
X distance from the low impedance end.

The analytical solution for the reflection coefficient along a lossless exponentially tapered transmission line has been formulated by Womack [6]. At $X = 0$ the corrected expression[1] can be simplified to

$$r(0) = \frac{-2\gamma}{\delta} + \frac{A}{B} \tag{2}$$

where $r(0)$ is the reflection coefficient at the start of the line, and

$$A^2 = 1 + 4\gamma^2/\delta^2 \tag{3}$$

$$B = \frac{A + [r(l) + 2\gamma/\delta] \tanh(\delta A l/2)}{A \tanh(\delta A l/2) + r(l) + 2\gamma/\delta} \tag{4}$$

$$\gamma = j\beta = j(2\pi/\lambda) \tag{5}$$

l = length of taper

and $r(l)$ is the reflection coefficient at the load (high impedance) end of the taper.

The reflection coefficient $r(l)$ is readily obtained from Z_0 and Z_2 (refer to Fig. 1). The taper rate δ is obtained from (1) at $X = l$:

$$Z_2 = Z_1 \exp(\delta l) \tag{6}$$

or

$$\delta = (1/l) \ln(Z_2/Z_1). \tag{7}$$

The input impedance at the low impedance end of the tapered line can then be calculated using

$$Z_{in} = Z_1 \frac{1 + r(0)}{1 - r(0)}. \tag{8}$$

The inputs for (8) are therefore Z_1, Z_2, Z_0, l, and λ.

It is convenient to substitute the electrical length θ into the previous equations thereby normalizing the parameters to frequency. Performing this substitution in (2)–(5) yields

$$r(0) = -C + A/B \tag{9}$$

$$A^2 = 1 + C^2 \tag{10}$$

$$B = \frac{A + [r(l) + C] \tanh(AD/2)}{A \tanh(AD/2) + r(l) + C} \tag{11}$$

$$C = j2\theta/D \tag{12}$$

$$D = \ln(Z_2/Z_1). \tag{13}$$

Thus the required inputs to (8) have been reduced to Z_1, Z_2, Z_0 and θ, only. This effectively generalizes the solution to any frequency of application and transformation ratio of interest.

The input impedance Z_{in} was calculated for several transformation ratios (Z_2/Z_1) and for a range of electrical lengths of the taper with $Z_2 = Z_0$.[2] The results are shown in Fig. 2. The abscissa is the real part of the input impedance, and the ordinate is the imaginary part of the input impedance, both normalized to Z_0. Each of the solid lines corresponds to a fixed ratio of Z_2/Z_1; its value is shown in the small spiral at the left hand end of each line. The broken lines correspond to fixed values of electrical length. It was not practical to indicate lengths above 120°, but the behavior of a typical case up to several wavelengths in length is shown in Fig. 3.

Manuscript received March 18, 1974; revised June 10, 1974.
The authors are with the Semiconductor Research and Development Laboratory, Motorola, Inc., Phoenix, Ariz. 85008.

[1] The original solution given by Womack contained sign errors.
[2] $Z_2 \neq Z_0$ gives no cases of comparable interest.